

Period-adding bifurcations and chaos in a periodically stimulated excitable neural relaxation oscillator

S. Coombes and A. H. Osbaldestin

Nonlinear and Complex Systems Group, Department of Mathematical Sciences, Loughborough University, Leicestershire LE11 3TU, United Kingdom

(Received 14 March 2000; revised manuscript received 22 May 2000)

The response of an excitable neuron to trains of electrical spikes is relevant to the understanding of the neural code. In this paper, we study a neurobiologically motivated relaxation oscillator, with appropriately identified fast and slow coordinates, that admits an explicit mathematical analysis. An application of geometric singular perturbation theory shows the existence of an attracting invariant manifold, which is used to construct the Fenichel normal form for the system. This facilitates the calculation of the response of the system to pulsatile stimulation and allows the construction of a so-called extended isochronal map. The isochronal map is shown to have a single discontinuity and be of a type that can admit three types of response: mode-locked, quasiperiodic, and chaotic. The bifurcation structure of the system is seen to be extremely rich and supports period-adding bifurcations separated by windows of both chaos and periodicity. A bifurcation analysis of the isochronal map is presented in conjunction with a description of the various routes to chaos in this system.

PACS number(s): 87.10.+e, 05.45.Xt

I. INTRODUCTION

The formulation of analytically tractable models of synaptically interacting neurons is of fundamental importance in the understanding of the behavior of biological neural systems. Many biologically realistic models of the single neuron, such as the Hodgkin-Huxley model, are so complex that they provide little intuitive insight into the dynamics they simulate, especially at the network level. Extracting the essence of neuronal behavior has encouraged many to pursue studies of networks of simple interacting threshold elements. The simplest and most thoroughly understood is the binary Hopfield model [1]. At the network level this has proved extremely useful in providing metaphorical models of learning and memory retrieval at the expense of maintaining contact with biological reality. Cells in the Hopfield model are described as either firing or not firing and do not have the capability of describing variations in neuronal firing rates, and neither are delays arising from the synaptic transmission process or the propagation of action potentials allowed for. The consideration of neurons as threshold devices for generating trains of spikes that can induce realistic postsynaptic potentials in other neurons has led to detailed studies of integrate-and-fire neural networks (see [2] for a recent review). In these models, the properties of dendrites, axons, and synapses are described with the use of an appropriately defined, yet biologically realistic, delay kernel, and the time of generation of a spike is considered to be all important. These systems are having increasing success in modeling aspects of biological neural systems ranging from the generation of locomotor patterns [3] to the understanding of orientation tuning in the visual cortex [4]. Undoubtedly, there will be some instances in which the use of an integrate-and-fire or related model is inappropriate. One such instance has arisen recently that is related to the response of isolated single neurons to trains of repetitive pulsatile stimuli. It is known from several studies that with variation in the period

of pulsatile stimulation, an alternating pattern of period and chaotic response can be observed in a single excitable neuron [5–9]. In fact, it is possible to observe a period-adding bifurcation interspersed with windows of chaos. Such behavior has been reproduced, to some extent, with complex models combining the Hodgkin-Huxley equations with calcium and calcium-dependent potassium components [10–13]. In a recent study of the periodically forced integrate-and-fire neuron, no such response was found [14]. The integrate-and-fire neuron focuses on the generation of action potentials or spikes and makes no attempt to mimic their electrical wave forms. It is likely that this is the source of their inability to reproduce experimentally observed behavior under repetitive pulsatile stimulation. Motivated by this discrepancy, we turn to another less studied model of a single neuron related to the binary model originally introduced by Abbott [15]. The binary model of Abbott belongs to the class of mathematical systems known as planar relaxation oscillators. One may regard it as either a caricature of the Hodgkin-Huxley system or a generalization of the integrate-and-fire model to incorporate a state-dependent threshold and a representation of a spike. In either case, we shall demonstrate that it is an analytically tractable single neuron model that can produce period-adding bifurcations with windows of both chaos and periodicity that submits to an exhaustive analysis within the framework of dynamical systems theory. Previous studies of periodically driven relaxation oscillators have focused upon numerical studies in the so-called oscillatory regime, where the system supports a limit cycle in the absence of any external signal [16–18]. Systems with limit cycles may be quite naturally investigated at the network using such techniques as averaging theory that allow one to use theories developed for the study of coupled oscillators (see, for example, [19]). One may also invoke the use of phase-response curves and isochronal coordinates to study the behavior of such systems to external forcing [20,21]. Interestingly, in the case of the oscillatory FitzHugh-Nagumo model, both period-adding bifurcations and irregular activity have been

observed numerically [22], suggesting that mathematical studies of planar relaxation oscillators under pulsatile stimulation should be pursued. It is important to appreciate, however, that many neurons function as excitable threshold elements. Typically they will only elicit a single spike of electrical activity in response to a pulsatile stimuli of sufficient magnitude. Studies of excitable systems under pulsatile stimulation are relatively few compared to their oscillatory counterparts. A recent paper on the bifurcation structure of a periodically forced nerve pulse equation modeling cardiac conduction redresses this balance somewhat [23]. Importantly, it has been established that some of the techniques for dealing with oscillatory systems may be taken over to the excitable regime. Notably, work by Rabinovitch *et al.* extends the concept of isochronal coordinates to excitable systems with specific application to the forced Bonhoeffer–van der Pol oscillator in its excited mode [24,25]. This has been extended to the case of neural systems by Ichinose *et al.* [26] and Yoshino *et al.* [27]. In the first case, the authors numerically study the response characteristics of the excitable FitzHugh-Nagumo system. Bifurcations of the system are explained in terms of a mathematical idealization, the so-called Z model, a piecewise differentiable relaxation oscillator with a single stable node. The work of Yoshino *et al.* also pursues an investigation of the FitzHugh-Nagumo system, but this time it discusses a mathematical idealization of the expected isochronal map that includes the effects of a stable focus (rather than a stable node). In this paper, we show that one can make similar progress without recourse to oversimplification if one works directly with a piecewise linear caricature of the FitzHugh-Nagumo system known as the McKean model [28]. Within the context of excitable nerve tissue, this particular caricature has exact solutions associated with traveling pulses. In the limit that the fast and slow time scales of this system become effectively independent, one recovers the binary model of Abbott. In this paper, we consider the McKean model in the limit of weak dependence between the two-time scales of the system and utilize some of the framework of the binary model in the construction of isochronal coordinates under external pulsatile stimulation. By analyzing the properties of this map, we establish the conditions under which period-adding bifurcations and windows of chaos are to be found in the excitable McKean model under external periodic pulsatile stimulation.

In more detail, the outline of the paper is as follows. In Sec. II, we discuss planar relaxation oscillators appropriate for studying excitable nerve tissue and introduce the McKean model. The relationship to the binary model of Abbott is explained and the (state-dependent) threshold for a spike response is identified. We define the extended isochron of an excitable system with a stable node in Sec. III. With this definition we first show how to construct the isochronal map of the binary model under external pulsatile stimulation. The analysis of the resulting map predicts that the system can mode-lock to an external periodic pulsatile signal and undergo period-adding bifurcations but that it is unlikely to generate any chaotic orbits. In Sec. IV, we consider the less restrictive case in which the fast and slow time scales of the McKean model are weakly dependent. Using geometric singular perturbation theory, we show the persistence of invariant manifolds from the binary model. This allows us to cal-

culate estimates for the isochronal coordinates of the McKean model, which reduce to those of the binary model in some limit. With a mixture of numerics and analysis, the resulting isochronal map is shown to support an extremely rich bifurcation structure. Our main observation is the existence of period-adding bifurcations separated by windows of chaos and periodicity. The properties of the isochronal map responsible for this bifurcation structure are identified. Finally, in Sec. V we discuss the extension of the work presented in this paper to the important problem of synaptically coupled neural systems.

II. THE MODEL

The behavior of neural cells is often explored by examining the response of their cell membrane potential to the injection of an external current. These responses are partially dependent upon membrane conductance properties and the reversal potentials of the ions involved in generating the electrical response. Mathematical models for such processes are often given by combining current conservation with differential equations for the cell conductances and membrane potential. Perhaps the most famous model of nerve tissue is the Hodgkin-Huxley system [29]. Although originally introduced to model the squid giant axon, recent work suggests that the FitzHugh-Nagumo (FHN) model actually provides a better qualitative description [30]. This may seem somewhat surprising since the FitzHugh-Nagumo model is often considered as a two-dimensional caricature of the four-dimensional Hodgkin-Huxley dynamical system. Apart from this recent observation, one often prefers to study the FHN system for its comparative mathematical simplicity. The FitzHugh-Nagumo system is given by

$$\epsilon \dot{v} = f(v) - w - w_0 + I, \quad (1)$$

$$\dot{w} = v - \gamma w - v_0, \quad (2)$$

where $f(v) = Cv(v - \alpha)(1 - v)$. The variable v corresponds to membrane potential while w is associated with the refractory properties of a neuron. The parameters C , α , ϵ , w_0 , v_0 , and γ may be considered as combinations of the membrane reversal potentials and conductance properties while I is any externally injected current. For $\epsilon \ll 1$, one may regard the FHN system to be comprised of a fast variable, v , and a slow variable, w . The fast variable has a cubic nullcline ($\dot{v} = 0$) and the slow one has a nullcline ($\dot{w} = 0$) that is monotonically increasing. In this paper, we consider the piecewise linear caricature of the FHN nonlinearity, namely

$$f(v) = \begin{cases} -v, & v < \alpha/2 \\ v - \alpha, & \alpha/2 < v < (1 + \alpha)/2 \\ 1 - v, & v > (1 + \alpha)/2. \end{cases} \quad (3)$$

This choice is preferable for two reasons: (i) piecewise linear models often possess explicit solutions and (ii) the essential feature of the cubic nonlinearity in the FHN system is its ‘‘N’’ shape [15] and this is duplicated by the piecewise linear form with its negative resistance region. The above choice of nonlinearity was first considered by McKean [28] in the context of traveling nerve impulses, where it proved possible to

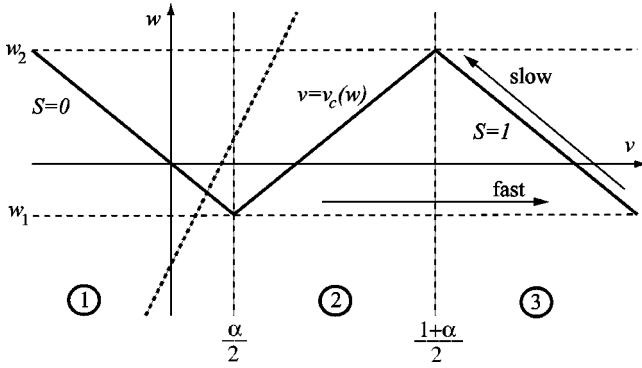


FIG. 1. The phase plane for the McKean model has a nullcline with an N shape (thick solid lines) corresponding to $\dot{v}=0$ and a linear one associated with $\dot{w}=0$ (thick dashed lines). The state-dependent threshold function is the middle part of the $\dot{v}=0$ nullcline described by the linear equation $v=v_c(w)$. In this figure the stable excitable fixed point lies at the intersection of the two nullclines on the $S=0$ branch.

calculate the speed and shape of traveling pulses exactly. The system has nullclines defined by $f(v)=w+w_0-I$ and $w=(v-v_0)/\gamma$. The case when the fixed point is such that $v < \alpha/2$ is said to define the excitable regime. It is convenient to keep track of which branch of the nonlinear function (3) is playing a role in the dynamics. To do this, it is natural to introduce the binary variable:

$$S = \begin{cases} +1, & v > (1+\alpha)/2 \\ 0, & v < \alpha/2. \end{cases} \quad (4)$$

If the time scale for the v dynamics is fast compared to the time scale for the w dynamics (i.e., in the limit as $\epsilon \rightarrow 0$), then v spends no appreciable time off of the nullclines for $\dot{v}=0$ and we may write $f(v)=S-v$. Introducing $S^+(t) = \lim_{\delta \rightarrow 0^+} S(t+\delta)$, we may write the dynamics for $S(t)$ in the form

$$S^+ = \Theta[I - w_0 + (S - \alpha)/2 - w], \quad (5)$$

where $\Theta(x)=1$ if $x \geq 0$ and is zero otherwise. To establish the validity of Eq. (5), we refer to Fig. 1 and check that S switches from 0 to 1 as w decreases through w_1 and that this is reversed as w increases through w_2 . The points w_1 and w_2 in Fig. 1 are easily calculated as $I - w_0 - \alpha/2$ and $I - w_0 - \alpha/2 + 1/2$, respectively. On the branches $S=0$ and 1, the evolution of v may be expressed as

$$v = S - w - w_0 + I. \quad (6)$$

This allows us to rewrite the slow dynamics in the form

$$\dot{w} = -\beta w + A + S, \quad (7)$$

where $\beta=1+\gamma$ and $A=I-w_0-v_0$. The fixed point (v^*, w^*) is given by $w^*=(v^*-v_0)/\gamma$ with

$$v^* = \frac{1}{\gamma+1} [\gamma(w_0 - I + X) - v_0], \quad (8)$$

where $X=S$ if the fixed point lies on one of the two branches $S=0$ or 1 (excitable regime) and $X=\alpha$ otherwise (oscilla-

tory regime). Up to a trivial rescaling, Eqs. (5) and (7) define the binary model originally introduced by Abbott [15]. The model is particularly appropriate for the modeling of oscillatory, plateau, and rebound properties of real neurons and has been useful in understanding models of networks of pulse-coupled neural relaxation oscillators. Insight into the latter system has come from both a mean-field analysis and a study of a single binary neuron under periodic square-wave stimulation. The response of the binary neuron model to repetitive pulsatile stimulation has not previously been performed. In the next section, we show how one may develop such an analysis with the use of isochronal coordinates.

III. ISOCHRONAL COORDINATES $\epsilon=0$

First let us focus on the binary model valid for $\epsilon=0$. In this case the system spends all of its time on the branches $S=0$ and 1. Following the work of Rabinovitch [24,25] and later work by Ichinose *et al.* [26] and Yoshino *et al.* [27], we define an extended isochron as a set of states synchronously approaching an asymptotically stable fixed point. The isochronal coordinate, $\tau(w, S)$, with an origin at $(v, w) = ((1+\alpha)/2, w_2)$, is considered to be the difference $t[(v, w) \rightarrow (v^*, w^*)] - t[((1+\alpha)/2, w_2) \rightarrow (v^*, w^*)]$, where $t[(v_1, w_1) \rightarrow (v_2, w_2)]$ denotes the time taken to move from (v_1, w_1) to (v_2, w_2) . Hence,

$$\tau(w, S) = \begin{cases} T, & S^+ = 1 \\ -T, & S^+ = 0, \end{cases} \quad (9)$$

where T is the time taken for the system to evolve from w to w_2 . The time taken to evolve onto a branch is considered to be essentially zero. We shall explore the consequences that a nonzero evolution time has shortly. By integrating Eq. (7), we may write the isochronal coordinate in the form

$$\tau(w, S) = \frac{1}{\beta} \ln \left[\frac{w_2 - (S+A)/\beta}{w - (S+A)/\beta} \right] (-1)^S. \quad (10)$$

One of the useful properties of isochronal coordinates is that the following equality holds if there is no stimulation between t and $t+\Delta$:

$$\tau(w(t+\Delta), S(t+\Delta)) = \tau(w(t), S(t)) + \Delta. \quad (11)$$

We now consider a train of pulsatile stimulation at times t_n such that $v \rightarrow v + \kappa_n$ when $t = t_n$. Assuming $w_1 < w < w_2$, we may write

$$S_n^+ = \Theta(v + \kappa_n - v_c(w)), \quad (12)$$

where $S(t_n) = S_n$ and $v_c(w)$ is defined by the condition $\dot{v} = 0$ and $f(v) = v - \alpha$, which gives $v_c(w) = w + \alpha + w_0 - I$. Hence, using Eq. (6) (under the assumption that just before the stimuli the system lies on one of the branches $S=0$ or 1), Eq. (12) may be written in the form

$$S_n^+ = \Theta(S_n - h(w, \kappa_n)), \quad (13)$$

where $h(w, \kappa)$ is defined by

$$h(w, \kappa) = 2w + \alpha - \kappa - 2(A + v_0). \quad (14)$$

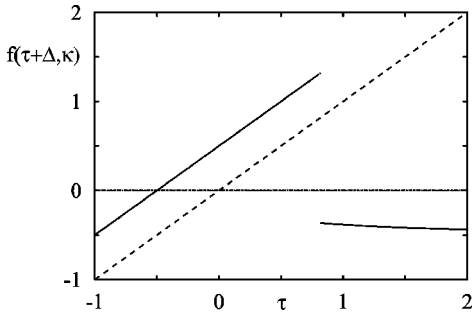


FIG. 2. The graph associated with the isochronal map for the case $\epsilon=0$. Other parameters are $I=v_0=w_0=0$, $\alpha=0.25$, and $\gamma=\Delta=0.5$.

For simplicity, we shall assume that the period of stimulation is sufficiently large so as to allow the system to relax back to the $S=0$ branch between stimuli. In this case, we have that

$$\tau(w_{n+1}, 0) = \tau(w_n, S_n^+) + \Delta_n, \tag{15}$$

where $w_n = w(t_n)$ and $\Delta_n = t_{n+1} - t_n$. Now the isochronal coordinate on the $S=0$ branch is given by Eq. (10) with $S=0$ so that on this branch $w_{n+1} = \Psi(\tau(w_{n+1}, 0))$:

$$\Psi(\tau) = \frac{1}{\beta} [A + \phi \exp(-\beta\tau)] \tag{16}$$

with $\phi = \beta[w_2 - A/\beta]$. The isochronal coordinate $\tau(w_{n+1}, S_{n+1}^+)$ just after the next stimulation may be calculated from Eq. (10), and using Eqs. (15) and (16) allows us to write

$$\tau_{n+1} = f(\tau_n + \Delta_n, \kappa_n), \tag{17}$$

where $\tau_n = \tau(w_n, S_n^+)$ and

$$f(\tau, \kappa) = \begin{cases} f_L(\tau, \kappa) \equiv \tau, & \kappa < \kappa_c(\tau) \\ f_R(\tau, \kappa) \equiv \frac{1}{\beta} \ln \left[\frac{1 - \phi}{1 - \phi e^{-\beta\tau}} \right], & \kappa > \kappa_c(\tau). \end{cases} \tag{18}$$

The threshold condition in the isochron map is determined by $h(\Psi(\tau), \kappa) = 0$ so that

$$\kappa_c(\tau) = 2\Psi(\tau) + \alpha - 2(A + v_0). \tag{19}$$

An example of the graph of the function (18) is shown in Fig. 2.

Period-adding bifurcations

From now on we examine the case that $\Delta_n = \Delta$ and $\kappa_n = \kappa$ for all n . It is straightforward to show that $f'(\tau, \kappa) < 0$ for $\kappa > \kappa_c(\tau)$ so that in the limit of a large number of iterations bounded dynamics is confined to an invariant interval $\Sigma_\tau = [\sigma_L, \sigma_R]$ with $\sigma_L = f_R(\tau_c + \Delta, \kappa)$ and $\sigma_R = f_L(\tau_c + \Delta, \kappa)$. The quantity τ_c is given by the solution of $\kappa_c(\tau_c) = \kappa$. It is convenient to introduce a new coordinate $x = g(\tau) = (\tau - \sigma_L) / (\sigma_R - \sigma_L)$. The dynamics in this new variable is given by $x_{n+1} = h(x_n)$ with

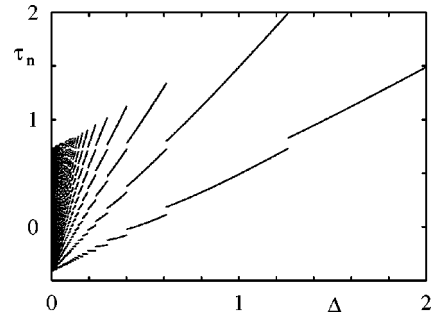


FIG. 3. The period-adding bifurcation scenario for the isochronal map as a function of the stimuli period Δ . Parameters are $I=v_0=w_0=0$, $\alpha=0.25$, $\gamma=0.5$, and $\kappa=0.5$.

$$h(x) = \begin{cases} h_L(x) \equiv g \circ f_L \circ g^{-1}(x + \Delta), & x < \theta \\ h_R(x) \equiv g \circ f_R \circ g^{-1}(x + \Delta), & x > \theta \end{cases} \tag{20}$$

for some parameter $\theta = g(\tau_c) \in (0, 1)$. Note that the invariant interval is now $\Sigma_x = [h_R(1), h_L(\theta)] = [0, 1]$. For realistic parameter values it is always possible to establish the following properties: (i) $h'_L(x) > 0$ and $h'_R(x) < 0$ for all θ , (ii) $h_R(\theta) < h_L(0)$, (iii) $h_L(x) > x$ for all $x \leq \theta$, and (iv) $|h'(x)| \leq 1$. It has been rigorously shown by LoFaro [31] that such maps allow only period n and period $n + 1$ orbits to coexist, both of which are attracting. Moreover, as θ is increased, the system bifurcates from a single period n orbit to the coexistence of a period n orbit with a period $n + 1$ orbit and then to a single period $n + 1$ orbit. Period-adding bifurcations are therefore expected as we vary Δ for the isochronal map (17) and are indeed those observed in numerical simulations (see Fig. 3). We shall refer to periodic orbits of order n as being $1:n$ mode-locked since the response of the system repeats after n applications of the (periodic) external stimulus. In the limit of small ϵ , and under periodic pulsatile stimulation, the coexistence of periodic attractors has also been observed numerically in systems of the type described by Eqs. (1) and (2) when $f(v)$ has the cubic shape of the Bonhoeffer-van der Pol oscillator [18].

It is natural to define an excitation number ρ for the system as

$$\rho(\tau_0) = \lim_{N \rightarrow \infty} \frac{1}{N} \sum_{n=1}^N S_n^+ \tag{21}$$

This gives a measure of the average firing rate of the model neuron, an example of which is shown in Fig. 4. The char-

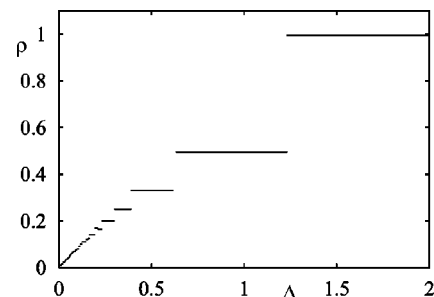


FIG. 4. Rotation number ρ (independent of τ_0) for the bifurcation diagram shown in Fig. 3.

acteristics of the excitation numbers of the binary model reveal a staircase structure with no chaotic response. In the next section, we show that the possibility of an incomplete devil's-staircase-like structure and the appearance of chaotic orbits are associated with a nonzero value for ϵ . Corrections to the instantaneous approximation of the binary model are calculated using geometric singular perturbation theory, which then allows the construction of an isochronal map along similar lines to those just presented.

IV. ISOCHRONAL COORDINATES $\epsilon \neq 0$

We have seen in the preceding section that the McKean model possesses a simplified structure on taking the singular limit $\epsilon \rightarrow 0$. The solution of this simplified system (usually referred to as an *outer* solution) is often a valid asymptotic expansion of the full system upon taking ϵ to be a small parameter. However, in some regions, such as near the nullclines of the fast variable, one would expect the appearance of a boundary layer. One technique for matching so-called *inner* solutions (valid in the neighborhood of a boundary layer) with outer solutions is the *method of matched asymptotics*. For the extension of the binary model to nonzero ϵ , one would expect boundary layers to develop in some small neighborhood of the branches $S=0$ and 1 as well as the threshold $v=v_c(w)$. In effect, for nonzero ϵ , one can no longer separate the dynamics of the fast and slow variables in all regions. This complicates the calculation of the times to evolve onto and off the branches $S=0$ and 1, necessary for the formulation of an isochronal map. The techniques of matched asymptotics allow such calculations for small $|\epsilon|$. Even though the McKean model is in fact exactly soluble, one must be prepared to deal with approximate solutions of a set of transcendental equations for the evolution times with this approach. For the purposes of this paper, it is more appropriate to use a complementary set of techniques developed using ideas from dynamical systems theory, known as the method of *geometric singular perturbation theory*. The full theory is often referred to as Fenichel theory and a review of those parts that we use in this section may be found in the tutorial article by Hayes *et al.* [32]. The theory is best applied when one can identify *good* fast and slow coordinates in a dynamical system. This facilitates the derivation of the so-called Fenichel normal form for the vector fields near their center manifolds (outer solutions), which explicitly contain the center dynamics and the exponential attraction (or repulsion) in forward time toward the center (slow) manifold.

When $\epsilon=0$, the McKean model possesses an invariant manifold which may be written in the form $v=m_0(w)$, with

$$m_0(w) = \begin{cases} m_0(w;0), & v < \alpha/2 \\ v_c(w), & \alpha/2 < v < (1+\alpha)/2 \\ m_0(w;1), & v > (1+\alpha)/2 \end{cases} \quad (22)$$

and $m_0(w;S)=S-w-w_0+I$. Note that for $\epsilon=0$, the two outer branches defined by $S=0$ and 1 are attracting while the inner branch defined by $v=v_c(w)$ is repelling. To establish that these statements are also true for small ϵ , it is convenient to first write the dynamics in terms of a second-order differential equation:

$$\epsilon \dot{v} + [\gamma \epsilon - f'(v)] \dot{v} + [v - \gamma f(v)] + \Gamma = 0, \quad (23)$$

where $\Gamma = \gamma w_0 - \gamma I - v_0$. Using the piecewise linear function given by Eq. (3), we have that

$$\epsilon \dot{v} + (\gamma \epsilon + 1) \dot{v} + (1 + \gamma)v + \Gamma - \gamma S = 0 \quad \text{regions 1 and 3,} \quad (24)$$

$$\epsilon \dot{v} + (\gamma \epsilon - 1) \dot{v} + (1 - \gamma)v + \Gamma + \gamma \alpha = 0 \quad \text{regions 2,} \quad (25)$$

where for convenience we call region 1 the regime where $v < \alpha/2$, region 2 is where $\alpha/2 < v < (1+\alpha)/2$, and finally region 3 is where $v > (1+\alpha)/2$ (see Fig. 1). The structure of these systems motivates an analysis of

$$\epsilon \dot{v} + (\gamma \epsilon + A) \dot{v} + (1 + A\gamma)v + C = 0, \quad (26)$$

where $A = \pm 1$ and C is some constant. Further simplification is obtained by shifting v such that $v \rightarrow v + C/(1+A\gamma)$ so that we may drop the last term in Eq. (26). The leading-order outer equation for Eq. (26) is then

$$A \dot{v} + (1 + A\gamma)v = 0 \quad (27)$$

and the leading-order inner equation is found by introducing $s \equiv t/\epsilon$:

$$\frac{d^2 v}{ds^2} + A \frac{dv}{ds} = 0. \quad (28)$$

The structure of the inner and outer equations motivates the following new variables:

$$X = \epsilon[A \dot{v} + (1 + A\gamma)v], \quad Y = \epsilon v + Av. \quad (29)$$

With this choice of dependent variables, X is a fast variable and Y is a slow variable. Note that $X=0$ gives the outer equation while $\dot{Y}=0$ gives the inner equation. From Eq. (29), we may write v and \dot{v} in terms of X and Y :

$$v = \left(\frac{1}{\epsilon B - A^2} \right) X + \left(\frac{-A}{\epsilon B - A^2} \right) Y, \quad (30)$$

$$\dot{v} = \left(\frac{-A}{\epsilon(\epsilon B - A^2)} \right) X + \left(\frac{B}{\epsilon B - A^2} \right) Y, \quad (31)$$

and $B = 1 + A\gamma$. Equation (26) may now be rewritten in X and Y coordinates as

$$\begin{bmatrix} X' \\ Y' \end{bmatrix} = \begin{bmatrix} -\frac{A[\epsilon(B+1)-A^2]}{\epsilon B - A^2} & \frac{\epsilon^2 B}{\epsilon B - A^2} \\ -\frac{\epsilon(B+A\gamma)}{\epsilon B - A^2} & \frac{\epsilon B(A - \epsilon\gamma)}{\epsilon B - A^2} \end{bmatrix} \begin{bmatrix} X \\ Y \end{bmatrix}, \quad (32)$$

where $' \equiv d/ds$. After expanding in powers of ϵ , it is apparent that the above is in the form to which Fenichel theory applies, i.e., we may write

$$X' = \mathcal{F}(X, Y; \epsilon), \quad (33)$$

$$Y' = \epsilon \mathcal{G}(X, Y; \epsilon), \quad (34)$$

where

$$\mathcal{F}(X, Y; \epsilon) = \left[-A + \frac{B+1}{A} \epsilon + O(\epsilon^2) \right] X + \left[-\frac{B}{A^2} \epsilon^2 + O(\epsilon^2) \right] Y, \quad (35)$$

$$\mathcal{G}(X, Y; \epsilon) = \left(\frac{B}{A^2} + O(\epsilon) \right) X - \left(\frac{B}{A} + O(\epsilon) \right) Y. \quad (36)$$

The $\epsilon=0$ case of Eq. (32) possesses a normally hyperbolic invariant manifold $\mathcal{M}_0 \equiv \{(X, Y) | \mathcal{F}(X, Y; 0) = -AX = 0\}$. By Fenichel's persistence theorem there exists a function $m_\epsilon(Y)$ satisfying $m_\epsilon(0) = 0$, whose graph $\{(X, Y) | X = m_\epsilon(Y)\}$ is a slow (center) manifold for the system (32) that is tangent to the Y axis at $(0, 0)$. It is guaranteed that $\mathcal{M}_\epsilon = \{(X, Y) : X = m_\epsilon(Y)\}$ is $O(\epsilon)$ close to \mathcal{M}_0 . Introducing the Fenichel coordinate $b = X - m_\epsilon(Y)$, the system (32) has the normal form

$$\epsilon \dot{b} = B_\epsilon(b, Y)b, \quad (37)$$

$$\dot{Y} = \mathcal{G}(b + m_\epsilon(Y), Y; \epsilon) \quad (38)$$

with $B_\epsilon(b, Y) = -A + O(\epsilon)$. Since $A = +1$ describes dynamics close to the branches $S=0$ and 1 , we easily see that these branches are attracting while $A = -1$ for the threshold $v = v_c(w)$ and it is repelling. The existence of a Fenichel normal form, in terms of the fast and slow variables X and Y , tells us that we may only consider the slow variable Y as fixed if $|b(t)| > |\epsilon|$. (In fact, for this system this statement holds for $|b(t)| > |\epsilon|^2$ [32].) A simple underestimate for the time taken to evolve onto the branches $S=0$ and 1 can therefore be obtained by considering the Fenichel normal form (37) with $\dot{Y} = 0$. For each of the dynamical systems in regions 1, 2, and 3 we consider the case of small ϵ so that to a first approximation the Fenichel coordinate can be taken as $b = v - m_\epsilon(w)$ [with $m_0(w)$ given by Eq. (22)]. We then integrate Eq. (37) with $Y = w$ considered as fixed to obtain an estimate for the duration of a given trajectory. To estimate the time taken to evolve from an initial point with $b(0) > \epsilon$ onto an attracting part of the invariant manifold, we calculate the time of flight to within a distance $O(\epsilon)$ of the invariant manifold as

$$\tilde{T} = \frac{\epsilon}{A} \ln \frac{b(\tilde{T})}{b(0)}. \quad (39)$$

In deriving Eq. (39) we have assumed that the slow variable w remains fixed for $|b(t)| > \epsilon$. Obviously, a better estimate could be obtained by analyzing the full Fenichel normal form for the system with $\dot{b} = 0$ on the set $b = 0$, but this is not necessary for our purposes. We are now in a position to refine our construction of the isochronal coordinates by estimating the time spent evolving onto the invariant manifold that is ϵ close to the branches $S=0$ and 1 . In regions 1 and 3, we find

$$\tilde{T} = -\epsilon \ln[v - m_0(w, S)] + O(\epsilon \ln \epsilon) \quad (40)$$

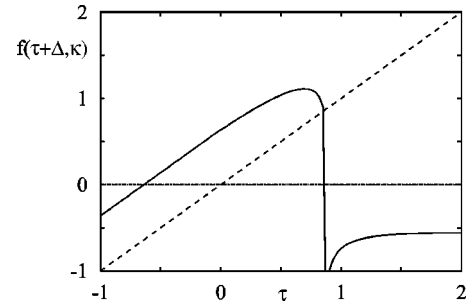


FIG. 5. The graph associated with the isochronal map for the case when $\epsilon = 0.2$ and $\Delta = 0.5$.

while for regions formed from the union of region 2 and region 1 or region 2 and region 3,

$$\tilde{T} = -\epsilon \ln \left| \frac{\left(\frac{S+\alpha}{2} - m_0(w, S) \right) \left(\frac{S+\alpha}{2} - v_c(w) \right)}{v - v_c(w)} \right|, \quad (41)$$

where we drop terms of $O(\epsilon \ln \epsilon)$. In Eq. (41) one should take $S = 1$ if attraction is to the manifold close to the $S = 1$ branch and $S = 0$ for attraction to the manifold close to the $S = 0$ branch.

For small (but nonzero) ϵ , the isochronal map obtained from these estimates has the form of Eq. (17) with

$$f_L(\tau, \kappa) = \begin{cases} \tau - \epsilon \ln \kappa, & \kappa < \frac{\kappa_c(\tau)}{2} \\ \tau - \epsilon \ln \frac{\kappa_c(\tau)^2}{4[\kappa_c(\tau) - \kappa]}, & \frac{\kappa_c(\tau)}{2} < \kappa < \kappa_c(\tau), \end{cases} \quad (42)$$

$$f_R(\tau, \kappa) = \begin{cases} \frac{1}{\beta} \ln \left[\frac{1 - \phi_\epsilon}{1 - \phi_\epsilon e^{-\beta\tau}} \right] \\ -\epsilon \ln \frac{[\kappa_c(\tau) - 1]^2}{4[\kappa - \kappa_c(\tau)]}, & \kappa_c(\tau) < \kappa < \frac{1 + \kappa_c(\tau)}{2} \\ \frac{1}{\beta} \ln \left[\frac{1 - \phi_\epsilon}{1 - \phi_\epsilon e^{-\beta\tau}} \right] \\ -\epsilon \ln(\kappa - 1), & \kappa > \frac{1 + \kappa_c(\tau)}{2}, \end{cases} \quad (43)$$

where we make use of the fact that on the $S=0$ branch $w = \Psi(\tau(w, 0))$, where Ψ takes the form

$$\Psi(\tau) = \frac{1}{\beta} [A + \phi_\epsilon \exp(-\beta\tau)] \quad (44)$$

and $\phi_\epsilon = 4^\epsilon \phi$. Note that Eq. (44) reduces to Eq. (16) in the limit $\epsilon \rightarrow 0$ as expected. As for the $\epsilon = 0$ case, there is only one discontinuity in the isochronal map at $\tau = \tau_c$, where τ_c solves $\kappa = \kappa_c(\tau_c)$ and $\kappa_c(\tau)$ is given by Eq. (19) after using Eq. (44). An example of the graph of this new isochronal map (with nonzero ϵ) is given in Fig. 5. The shape of this map is remarkably similar to that of the isochronal map for the Z model, itself shown to be in remarkably good agreement with that obtained numerically from simulations of the

FitzHugh-Nagumo model with $\epsilon=0.2$ [26]. Using these observations as a guide, we would expect good correspondence between the dynamics of the full McKean model and its reduction to the isochronal map for similar choices of ϵ . For the numerical examples presented in the next section, we make the choice $\epsilon=0.2$ throughout.

Bifurcation structure

For convenience we rewrite the dynamics in the form $\tau_{n+1}=h(\tau_n)$, where

$$h(x)=\begin{cases} h_L(x)=f_L(x+\Delta,\kappa), & x<\theta \\ h_R(x)=f_R(x+\Delta,\kappa), & x>\theta \end{cases} \quad (45)$$

where the parameter θ is given by the solution of $\kappa_c(\theta+\Delta)=\kappa$. A numerical example of the bifurcation structures that one typically sees with variation in the stimuli period Δ for fixed stimuli strength κ is given in Fig. 6. The phenomenon of period adding is preserved for nonzero ϵ , albeit with the introduction of some new bifurcation structures, namely the appearance of windows in parameter space separating mode-locked orbits in which bifurcation structures not present in the $\epsilon=0$ case (binary model) are found. However, for small ϵ the bifurcation diagrams are essentially indistinguishable. One also sees from the evaluation of the associated excitation number (see Fig. 7) an incomplete *perturbed* devil’s-staircase-like structure, somewhat more complicated than that of the binary model. To establish whether any of the orbits are chaotic, we numerically evaluate the Liapunov exponent. The Liapunov exponent λ gives a measure of orbital stability and is defined as

$$\lambda(\tau_0)=\lim_{N\rightarrow\infty}\frac{1}{N}\sum_{n=1}^N\ln\left|\frac{d\tau_{n+1}}{d\tau_n}\right|. \quad (46)$$

In fact, the numerical evaluation of the Liapunov exponent (shown in Fig. 8) and rotation number (shown in Fig. 7) for the bifurcation data shown in Fig. 6 indicates the possibility of chaotic orbits, as well as showing regions in parameter space in which periodic or quasiperiodic motion occurs. It would appear that the absence of chaotic orbits in the binary model is an artifact of the singular limit $\epsilon=0$. The binary model is not sufficiently rich to exhibit chaotic behavior. For arbitrarily small values of ϵ , however, there are chaotic windows in the bifurcation diagram of the isochronal map, al-

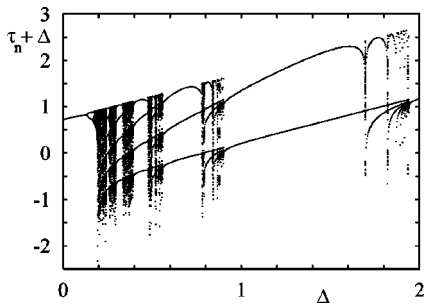


FIG. 6. The period-adding bifurcation scenario interspersed with chaotic windows for the isochronal map with nonzero ϵ as a function of the stimuli period Δ . Parameters are $I=v_0=w_0=0$, $\alpha=0.25$, $\kappa=0.5$, and $\epsilon=0.2$.

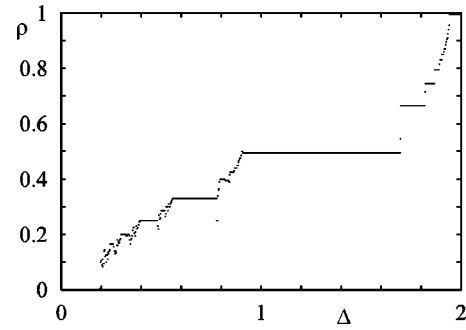


FIG. 7. Rotation number ρ for the bifurcation diagram shown in Fig. 6 (with $\tau_0=0.1$).

though their size may be small. The mechanisms for the generation of chaotic orbits will be outlined below. Other differences between the isochronal map derived in Sec. III and that derived using geometric singular perturbation theory include the fact that for $\epsilon=0$ the isochronal map has a finite invariant interval, while for nonzero ϵ it has a (semi)-infinite invariant interval. Also, since the gradient of the left-hand branch of the $\epsilon=0$ isochronal map is unity, it cannot have any fixed points in the limit $\Delta\rightarrow 0$, for which the attractor becomes a finite interval. For $\epsilon\neq 0$, it is simple to show that the derivative of the left-hand branch of the isochronal map is less than unity and that it possesses a stable fixed point as $\Delta\rightarrow 0$. A nonzero ϵ also leads to new bifurcation structures including *windows* of parameter space that separate $1:n$ and $1:n+1$ mode-locked solutions, observed with decreasing Δ . As well as supporting a form of period-doubling bifurcation, the isochronal map with nonzero ϵ also supports period-adding and saddle-node (tangent) bifurcations.

For small values of Δ not too close to zero (referring to Fig. 6), the period-adding scenario, observed in Fig. 3 for the binary model, is preserved to some extent, but the bifurcation structure is not so easily described. As an illustrative example, we first focus on the right-hand side of Fig. 6. In Fig. 9, we show the bifurcations that occur between a $1:2$ and a $1:1$ mode-locked solution. The window of bifurcations that separates these mode-locked solutions is also seen to support a period-adding scenario, but for increasing Δ . For large Δ , the sequence of bifurcations ends with the appearance of a stable fixed point via a saddle-node bifurcation. Interestingly, the period-adding bifurcations appear to have some transition regime which is not quite sharp. In fact, these transition regimes have bifurcation structure all their own with both pe-

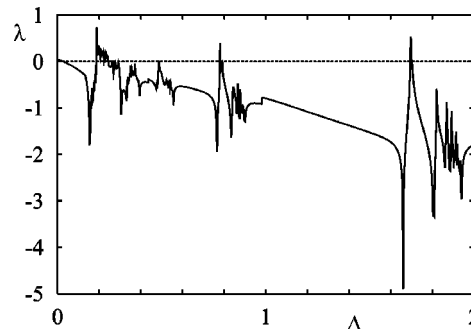


FIG. 8. Liapunov exponent λ for the bifurcation diagram shown in Fig. 6.

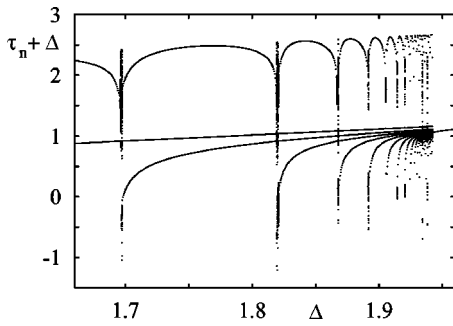


FIG. 9. A blowup of the bifurcation diagram shown in Fig. 6 showing a saddle-node bifurcation at around $\Delta=1.94$.

riod doubling and tangent bifurcations. An example of a period-doubling cascade in one of these transition regions is shown in Fig. 10. Such cascades occur at the *end* of each of the larger mode-locked intervals (which occur with increasing Δ). However, typically they themselves occupy a small window in parameter space and are unlikely to be of physical significance in neurodynamical systems. In the right-hand part of the bifurcation diagram (Fig. 10), this cascade ends abruptly with the appearance of a period-3 orbit. This qualitative change in behavior is associated with a tangent bifurcation. Note that before this tangent bifurcation (with increasing Δ), the invariant interval can become increasingly large and is infinite when $h_L(x_m) = \theta$, where x_m satisfies $h'_L(x_m) = 0$ and θ is the point at which the isochronal map has a discontinuity.

To establish that the bifurcation data in Fig. 6 are in some sense generic, we produce a numerical plot of the Liapunov exponent in the (Δ, κ) plane in Fig. 11. To help organize the form of these numerical data, we trace the locus of superstable cycles of $\tau_{n+1} = h(\tau_n)$ in Fig. 12. Superstable cycles of order p are defined as those points in parameter space for which both $h'(\tau) = 0$ and $\tau = h^p(\tau)$ for some integer p . Also, in Fig. 13 we trace the locus of period doubling and saddle-node bifurcation points for the map $\tau_{n+1} = h^p(\tau_n)$. A comparison of Fig. 11 with Figs. 12 and 13 shows that one can indeed organize much of the observed bifurcation structure of the isochronal map with this elementary analysis (especially outside the windows separating mode-locked orbits). The parameter regimes for nontrivial dynamical behavior can also be loosely identified by tracking the position of the fixed point. For example, in Fig. 6 the fixed point τ^* satisfies $h_R(\tau^*) = \tau^*$ for large Δ and is stable. Initially it is unstable,

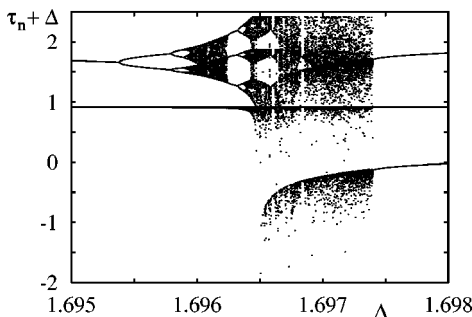


FIG. 10. A blowup of the bifurcation diagram shown in Fig. 6 showing a period-doubling bifurcation between $\Delta=1.695$ and 1.696.

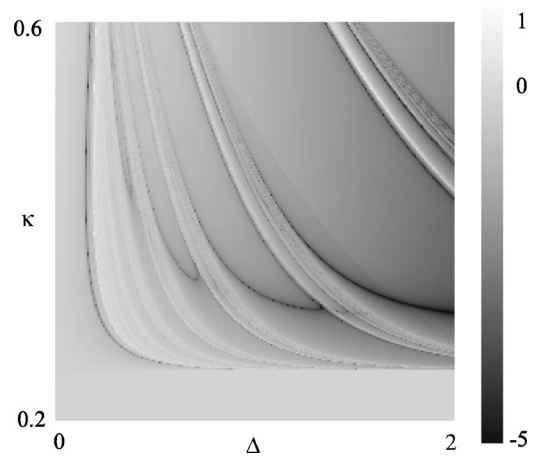


FIG. 11. Numerical evaluation of the Liapunov exponent λ for the (Δ, κ) parameter plane (for a 250×250 grid) with $\tau_0 = 0.1$, $\alpha = 0.25$, $\gamma = 0.5$, $\epsilon = 0.2$, and $I = v_0 = w_0 = 0$.

eventually becoming stable for small enough Δ . However, as Δ is decreased, the fixed point can fall upon the branch h_L . In the intermediate regime where $|h'_L(\tau^*)| > 1$, there may be parameter regimes which support a so-called snap-back repeller such that there exists at least one orbit starting from the vicinity of the unstable fixed point, which is repelled far away from the vicinity and then is *snapped* back to τ^* . The existence of such a repeller is sufficient for chaos [33]. Thus chaotic orbits may arise through at least two mechanisms, namely period-doubling cascades and the appearance of snap-back repellers. Some of the properties of the *windows* may also be uncovered without too much further work. For example, the shallow gradient of $h_R(\tau)$ for large τ underlies the narrowness (in parameter space) of the observed period-doubling cascades seen at the edge of a window that separates mode-locked solutions (see Fig. 10). As in numerical simulations of the Bonhoeffer–van der Pol oscillator, chaotic parameter regions are found to decrease with decreasing ϵ [18]. Moreover, similar bifurcation structures to those observed in the isochronal map derived from the McKean model, including the coexistence of periodic attractors, period-adding bifurcations, period-doubling bifurcations, and chaos, are seen. The precise scaling laws for the size of the chaotic windows are of mathematical interest, but perhaps not so important for a discussion of the computational properties of the McKean model and its usefulness in understanding data from real experiments such as those in [9]. It would

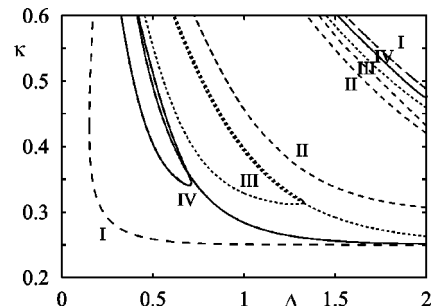


FIG. 12. Locus of superstable cycles of order 1 (I), 2 (II), 3 (III), and 4 (IV) in the (Δ, κ) plane corresponding to the parameters of Fig. 11.

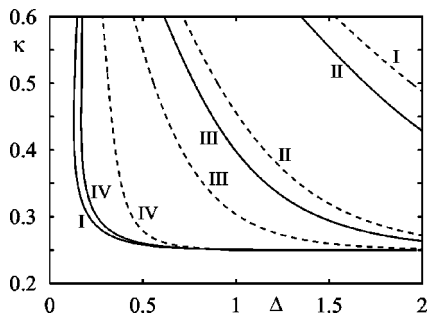


FIG. 13. Locus of period-doubling (solid lines) and saddle-node (dashed lines) bifurcations for the map $\tau_{n+1} = h^p(\tau_n)$, where $p = 1, \dots, 4$. The order of p in the figure is given in Roman numerals. Parameters are as for Fig. 11.

seem that period-adding bifurcations interspersed with chaotic activity are a feature of the McKean model, absent in the binary model ($\epsilon=0$). This is consistent with experimental observations of the behavior of real neurons and supports the credibility of the McKean model as a useful caricature of an excitable neuron.

V. DISCUSSION

In this paper we have shown that the response of the McKean model, of an excitable neuron, to pulsatile stimulation can be interpreted in terms of an associated discontinuous one-dimensional map, which we have called the extended isochronal map. This map is derived using techniques from geometric singular perturbation theory and previous definitions of isochronal coordinates for excitable systems. The parameter dependence of period adding, period doubling, and saddle-node bifurcations can be used to organize some of the rich structure observed in numerical experiments and to show that chaotic trajectories are suppressed in the limit that the voltage variable of the McKean model is much faster than the recovery variable. For small intervals between the application of pulsatile stimulation, we would not expect the dynamics of the isochronal map to approximate those of the full McKean model. In this case, the system would not have time to relax back to the state with $S=0$, violating one of the assumptions used in the reduction (the other being that we consider small ϵ). Hence, the period-adding bifurcation (seen with decreasing Δ) may be interrupted for small values

of Δ . In fact, numerical simulations of the FitzHugh-Nagumo system exhibit precisely this interruption and show a transition to a *superpulse* structure, where pulses are found superposed on one another [22]. However, for larger values of Δ one would expect the period-adding bifurcation to be seen. In experimental studies of cardiac tissue by Chialvo and Jaliffe [34], the bifurcation scenario $1:1 \rightarrow 1:2 \rightarrow 1:3 \rightarrow 1:4$ is clearly seen, suggesting that period-adding bifurcations are a feature of periodically stimulated excitable systems in general, not just neural ones. Chialvo and Jaliffe also make the observation that structures typically seen in periodically forced oscillatory systems, such as hierarchies of periodic solutions described by the Farey sequence, are possible in excitable systems. Similar conclusions may be drawn from our work by noting the devil's-staircase-like structure of the excitation number, also commonly seen in periodically forced oscillatory systems.

Importantly, the work presented applies to a generalization of the binary neuron model of Abbott [15] that can be explicitly analyzed in the presence of pulsatile stimuli. Since the output of such a neuron model can be used to specify a train of pulsatile stimuli [say, in the form of a spike train $\sum_n \delta(t - T^n)$, where the T^n are the times at which the isochronal coordinate passes through some reference value that signals a firing event, say $\tau=0$], one may easily formulate models of pulse-coupled McKean or binary neuron networks. Previous studies of coupled relaxation oscillators have focused upon coupling through fast threshold modulation [35,36] or variants thereof [37]. The extension of this approach to incorporate other caricatures of neural relaxation oscillators, which, for example, include the effects of stable foci or do not relax back near to rest between stimuli, is of course an area that should be developed. It is also likely that the extension to the case of noninstantaneous interactions may be possible using recent techniques developed by Yoshinaga *et al.* [38] for the study of synaptically coupled Hodgkin-Huxley equations. A program of work that includes features such as these as well as the effects associated with axonal, synaptic, and dendritic processing is a topic of current research.

ACKNOWLEDGMENT

S. C. would like to acknowledge support from the Nuffield Foundation.

-
- [1] J. J. Hopfield, Proc. Natl. Acad. Sci. USA **79**, 2554 (1982).
 - [2] P. C. Bressloff and S. Coombes, Neural Comput. **12**, 91 (2000).
 - [3] P. C. Bressloff and S. Coombes, Physica D **130**, 232 (1999).
 - [4] P. C. Bressloff, N. W. Bressloff, and J. D. Cowan, Neural Comput. (to be published).
 - [5] K. Aihara, G. Matsumoto, and M. Ichikawa, Phys. Lett. **111A**, 251 (1985).
 - [6] G. Matsumoto, K. Aihara, Y. Hanyu, N. Takahashi, S. Yoshizawa, and J. Nagumo, Phys. Lett. A **123**, 162 (1987).
 - [7] N. Takahashi, Y. Hanyu, T. Musha, R. Kubo, and G. Matsumoto, Physica D **43**, 318 (1990).
 - [8] D. T. Kaplan, J. R. Clay, T. Manning, L. Glass, M. Guevara, and A. Shrier, Phys. Rev. Lett. **76**, 4074 (1996).
 - [9] W. Ren, S. J. Hu, B. J. Zhang, and F. Z. Wang, Int. J. Bifurcation Chaos Appl. Sci. Eng. **7**, 1867 (1997).
 - [10] C. Kass-Petersen, *Bifurcations in the Rose-Hindmarsh and Chay Models*, in *Chaos in Biological Systems* (Plenum, New York, 1987), pp. 183–190.
 - [11] T. R. Chay, Physica D **16**, 233 (1985).
 - [12] A. V. Holden and Y. S. Fan, Chaos, Solitons and Fractals **2**, 221 (1992).
 - [13] Y. Fan and T. R. Chay, Biol. Cybern. **71**, 417 (1994).
 - [14] S. Coombes and P. C. Bressloff, Phys. Rev. E **60**, 2086 (1999).
 - [15] L. F. Abbott, J. Phys. A **23**, 3835 (1990).
 - [16] S. Sato and S. Doi, Math. Biosci. **112**, 243 (1992).
 - [17] B. Braaksma and J. Grasman, Physica D **68**, 265 (1993).
 - [18] S. Doi and S. Sato, Math. Biosci. **125**, 229 (1995).

- [19] F. C. Hoppensteadt and E. M. Izhikevich, *Weakly Connected Neural Networks*, Vol. 126 of Applied Mathematical Sciences (Springer-Verlag, New York, 1997).
- [20] A. T. Winfree, *The Geometry of Biological Time* (Springer-Verlag, New York, 1980).
- [21] A. Campbell, A. Gonzalez, D. L. Gonzalez, O. Piro, and H. Larrondo, *Physica A* **155**, 565 (1989).
- [22] D. Brown, J. P. A. Foweraker, and R. W. Marris, *Chaos, Solitons and Fractals* **5**, 359 (1995).
- [23] O. Kongas, R. von Herten, and J. Engelbrecht, *Chaos, Solitons and Fractals* **10**, 119 (1999).
- [24] A. Rabinovitch, R. Thieberger, and M. Friedman, *Phys. Rev. E* **50**, 1572 (1994).
- [25] A. Rabinovitch and I. Rogachevskii, *Chaos* **9**, 880 (1999).
- [26] N. Ichinose, K. Aihara, and K. Judd, *Int. J. Bifurcation Chaos Appl. Sci. Eng.* **8**, 2375 (1998).
- [27] K. Yoshino, T. Nomura, K. Pakdaman, and S. Sato, *Phys. Rev. E* **59**, 956 (1999).
- [28] H. P. McKean, *Adv. Math.* **4**, 209 (1970).
- [29] A. L. Hodgkin and A. F. Huxley, *J. Physiol. (London)* **116**, 449 (1952).
- [30] J. R. Clay and A. Shrier, *J. Theor. Biol.* **197**, 207 (1999).
- [31] T. LoFaro, *Math. Comput. Modell.* **24**, 27 (1996).
- [32] M. Hayes, T. J. Kaper, N. Kopell, and K. Ono, *Int. J. Bifurcation Chaos Appl. Sci. Eng.* **8**, 189 (1998).
- [33] H. Marotto, *J. Math. Anal. Appl.* **63**, 199 (1978).
- [34] D. R. Chialvo and J. Jalife, *Nature (London)* **330**, 749 (1987).
- [35] D. Somers and N. Kopell, *Biol. Cybern.* **68**, 393 (1993).
- [36] D. Somers and N. Kopell, *Physica D* **89**, 169 (1995).
- [37] G. Renversez, *Physica D* **114**, 147 (1998).
- [38] T. Yoshinaga, Y. Sano, and H. Kawakami, *Int. J. Bifurcation Chaos Appl. Sci. Eng.* **9**, 1451 (1999).